Liquid Crystals
Publication details, including instructions for authors and subscription information:
http://www.informaworld.com/smpp/title~content=t713926090

Critical radius of loop defects in homeotropic nematic liquid crystals

S. Thiberge; C. Chevallard; J. M. Gilli; A. Buka

Online publication date: 06 August 2010

To cite this Article Thiberge, S. , Chevallard, C. , Gilli, J. M. and Buka, A.(1999) 'Critical radius of loop defects in homeotropic nematic liquid crystals', Liquid Crystals, 26: 8, 1225 — 1234
To link to this Article: DOI: 10.1080/026782999204246
URL: http://dx.doi.org/10.1080/026782999204246

LIQUID CRYSTALS, 1999, VOL. 26, NO. 8, 1225–1234

Critical radius of loop defects in homeotropic nematic liquid crystals

S. THIBERGE*, C. CHEVALLARD, J. M. GILLI
Institut Non Linéaire de Nice, (U.M.R 129 C.N.R.S.) Université de Nice
Sophia–Antipolis, 1361, route des Lucioles, 06560 Valbonne, France

and A. BUKA
Research Institute for Solid State Physics of the Hungarian Academy of Sciences,
H-1525 Budapest, P.O. Box 49, Hungary

(*Received 12 August 1998; in final form 8 March 1999; accepted 15 March 1999*)

We describe an experimental situation with a looped line defect in nematic liquid crystals observed by polarizing optical microscopy. We measured the critical size of the loop below which it spontaneously shrinks and transforms into a point defect. The experiment was done with 5CB which gives rise to twist disclinations as do most of the usual nematics. For this kind of disclination an in-plane force due to the boundary conditions acts on the line and influences the critical radius. We have constructed a model which is in good agreement with experimental measurements and deduced the line tension of the disclination.

1. Introduction

Nematic liquid crystals are useful media in the study of the formation, structure, stability and dynamics of topological defects such as walls, lines (strings) and point singularities [1–4]. The special case of domain walls which separate regions with stable and metastable director configurations has attracted considerable interest [5, 6], since these states can easily be created in nematics by applying external fields. From general considerations, the motion of the defect will be determined by the elastic and external field energy difference between the two states, the viscous damping and the core (elastic) energy of the defect [7–9].

Concerning the case of a nematic between homeotropically anchored glass plates, different experimental situations allowing the observation of such line defects are described in reference [6]. In particular, a disclination is usually observed in the neighbourhood of curved interfaces separating the nematic from other materials (air, isotropic phase, metal wires, etc.) [8, 9]. The reason is that the curved profile of the interface and the anchoring conditions on it force a turn-over of the director across the sample thickness. Then a line separates a region of homeotropic orientation from a region with a turn-over (π-wall) of the director.

We describe in the following an original experimental situation with cylindrical symmetry in which the line possesses a looped shape. In that case, the line tension can balance the free energy of the inversion domain allowing a measurement of the line energy. A similar situation has been described in focal-conic smectic domains [10].

2. Experimental

Small droplets of the nematic liquid crystal 5CB produced by the technique described in [6] are sandwiched between parallel glass plates separated by spacers of thickness d. The resulting cylindrically symmetric droplets ('globules') have a disc-like shape (the axis is along z and the radius is R_g) with a concave meniscus along the side. The cross section of a globule is shown in figure 1. The director distribution indicated in the figure is a result of homeotropic anchoring on the glass plates achieved by lecithin coating and the natural

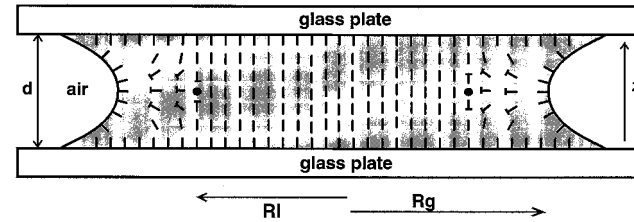

Figure 1. Schematic cross section of a globule with radius R_g. A loop defect of radius R_l is located in the midplane of the sample and is denoted by two black dots. Nails denote the out-of-plane director components.

*Author for correspondence; e-mail: thiberge@inln.cnrs.fr

perpendicular alignment of molecules at the nematic–air interface [11]. One can distinguish two regions: the central part of the globule which is homeotropic, and its outer ring in which the semi-toroidal shape of the meniscus imposes a π turn of the director along z. Then a singular line of topological charge $-1/2$ separates the two regions. Because of the cylindrical geometry the disclination line forms a circular loop of radius R_l (see figures 1 and 2).

Samples of thickness d (measured by conoscopic technique [12]) in the range 5–60 μm have been used. Measurements were carried out at room temperature (22°C) using a polarizing microscope equipped with a video camera. Pictures were recorded and digitized. An image analyser program was used to measure the line defect radius R_l and the position of the extinction brushes.

An image and a schematic representation of a globule between crossed polarizers are shown in figure 2. The central homeotropic region of the globule is surrounded by the disclination loop. The appearance of the outer region containing the deformed director profile (π turn along z) will be discussed below. It is bordered by the meniscus, which appears always as a black ring with or without polarizers. Its thickness (M) was typically found in the range 15–30 μm and showed only a weak d dependence. The outer black background in figure 2 (a) is the air around the globule and this also contains the meniscus.

3. The loop defect and the π wall

3.1. *General observations*

Depending on the radius of the globule R_g one finds two initial situations. First, in *large globules* the loop defect has a stable position at a distance S from the meniscus ($S = R_g - R_l$). S was found in the range 10–25 μm for our sample thickness range and was also only slightly d dependent. Applying an electric field across the sample, S decreases, and the line is pushed towards the meniscus. On switching off the field, the line relaxes to its equilibrium position with a characteristic time which is independent of the globule size in the limit of small curvature where the line tension can be neglected.

Since the liquid crystal 5CB has a positive diamagnetic anisotropy $\Delta\chi$, applying a rotating magnetic field **H** in the plane of the sample with an appropriate strength and rotation frequency (typically a few Hz), the radius of the defect line can be decreased and the defect can be positioned at any R_l. On removing the magnetic field, the defect loop either relaxes to its initial position at distance S from the meniscus if $R_l > R_l^c$, where R_l^c is the critical value of the defect radius, or it shrinks and implodes to a point defect of topological charge $+1$ in the middle of the globule if $R_l < R_l^c$. By applying both an electric field along z and a rotating magnetic field in the xy-plane, one can precisely control the position of the defect line.

Secondly, in *small globules*, the defect loop shrinks spontaneously and the stable configuration is a point defect ($R_l = 0$) in the centre of the globule, with a π wall in the midplane of the whole sample. One observes the extinction cross between crossed polarizers which is usually deformed into a spiral towards the globule boundary. The direction of the cross deformation—the handedness of the spiral—alters from globule to globule. In extremely small globules ($R_g \simeq 1$–$2d$) a perpendicular extinction cross without spiralling was observed, indicating a different, probably metastable, configuration

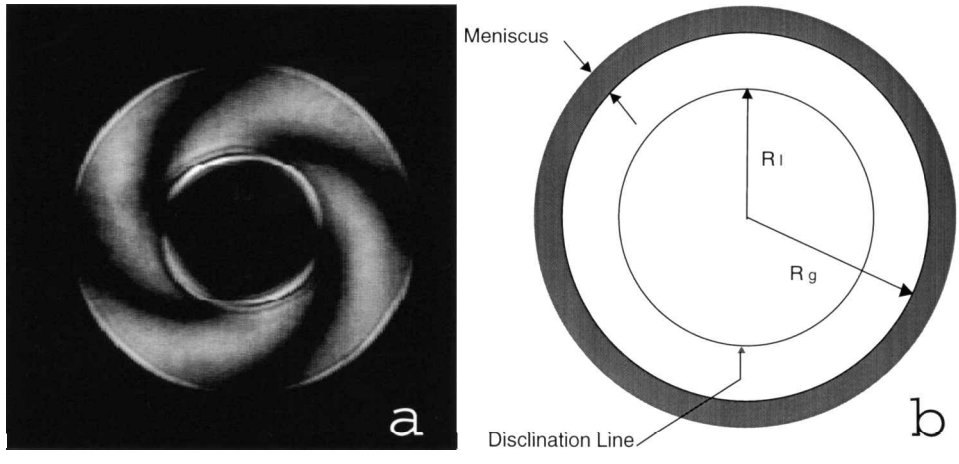

Figure 2. (a) A microscopic image of a globule observed between crossed polarizers. The central black region is homeotropic nematic and the external black area is air. In the intermediate region, there is a turn-over of the director along z. The disclination line is easily seen between the homeotropic and the distorted regions. The polarizers are horizontally and vertically oriented. The meniscus is not visible under crossed polarizers. (b) Schematic representation of the globule.

which is presumably due to the structure of the point defect [13].

Starting from a globule with a point defect in its centre, it is possible to generate the looped line configuration by applying a high voltage (explosion). The transition from a point defect to a looped line needs a high electric field of the order of 25 000 V cm^{-1}. Applying this field, the point defect explodes and the line rapidly approaches the globule boundary, breaking the anchoring at the meniscus. At this point, if the electric field is reduced to a few thousand V cm^{-1}, the natural anchoring at the meniscus is restored and the line reappears in the globule. In small globules the field must be sufficiently high to keep the line close to the meniscus.

If the field is switched off, the loop slowly shrinks (see the dashed line in figure 3). By applying an electric field during this process, one can influence the loop dynamics. Choosing a voltage (well below the explosion voltage) and switching it on at t_1 (early) the line motion reverses (as curve 1 shows). Applying it at t_3 (late), the line velocity decreases, but it continues to shrink (see curve 3). Repeating this experiment several times for a given applied voltage V, one can find with good accuracy the value of the critical radius $R_l^c(V)$ at which the defect is stationary (curve 2).

3.2. *Description of the director distribution*

Let us now consider the director distribution in the vicinity of the defect line. Ideally, the disclination line could be of the wedge or twisted type (see figure 4) [4]. Though the wedge disclination represents a simple director configuration (i.e splay–bend distortion in the plane perpendicular to the line), it is very rarely observed.

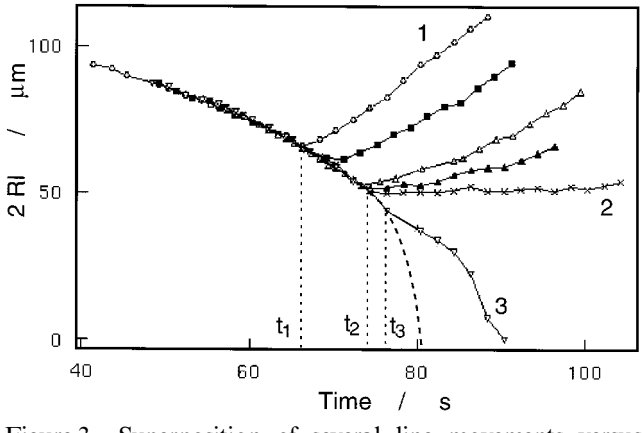

Figure 3. Superposition of several line movements versus time. The dashed curve shows spontaneous shrinking ($V = 0$) of the loop radius. Curves 1, 2 and 3 demonstrate the loop radius behaviour when a voltage V is applied at t_1, t_2 and t_3, respectively. $R_l^c(V)$ denotes the stationary loop radius for the given V.

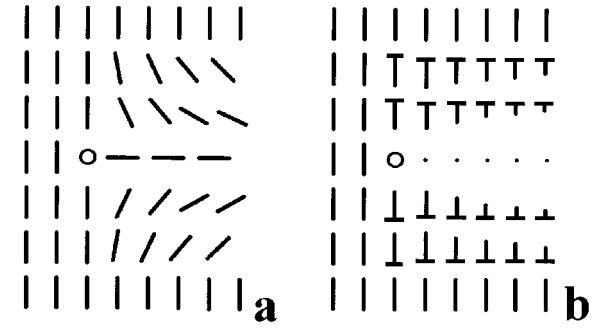

Figure 4. (*a*) A pure wedge disclination; (*b*) a pure twist diclination with homeotropic anchoring on the surfaces.

Instead, a more complex arrangement including twist is preferred in usual nematic liquid crystals. This is due to the difference in the elastic free energy densities associated with the three types of deformations. The wedge disclination would be stable if $K_2 \gg K_1$ or K_3. This is normally not the case for usual nematics, and contrarily, for $K_2 < K_1$ or K_3, the director escapes out of the splay–bend distortion plane into the third dimension. In this way the resulting configuration involves twist and consequently decreases the total energy. Anisimov and Dzyaloshinskii [14] have calculated the condition under which the elastic constants determine which configuration will be more favourable energetically. They showed that a wedge line in an infinite medium is unstable if $K_2 < (K_1 + K_3)/2$. This is also the case for 5CB (from [15] the ratios of K_i/K_1 are 1 : 0.5 : 1.3).

Experimental evidence for the fact that the disclination line in our globule (observed with 5CB) cannot be a pure wedge type is the spiral shape of the extinction cross, see figure 2(*a*); this indicates that the director prefers to approach the loop tangentially instead of radially. Thus the twisted structure shown in figure 4(*b*) is preferred against figure 4(*a*) in the vicinity of the line. The latter involves all three elastic deformations.

The director position will be described using cylindrical coordinates (r, ψ, z). Two angles θ and Φ are also introduced which describe the director orientation in a polar coordinate system; θ is the tilt angle and Φ the azimuthal angle (see figure 5). Under homeotropic anchoring, $\Phi = 0$ in a pure wedge disclination [see figure 4(*a*)] and $\Phi = \pi/2$ in a twist type disclination [see figure 4(*b*)].

The system we are studying is cylindrically symmetric; thus we do not consider ψ dependence. Let us take a line at the position R_1. For $r < R_1$ the director is homeotropically aligned ($\theta = 0$). For $r > R_1$, following the director variation along Oz, one has a splay–bend deformation described by the angle $\theta(r, z)$ (the π wall). One should note that θ is a function of z, but near the line it is also a function of r, because the thickness of the π wall tends to zero in the vicinity of the disclination line.

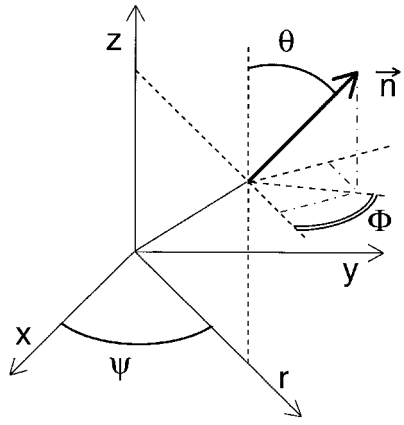

Figure 5. Coordinates system and notations of the director orientation.

In addition, a second deformation is present in the midplane of the sample at $z = 0$ containing the line. This deformation is due to the competition between the perpendicular anchoring at the meniscus ($\Phi = 0$) which would favour the wedge configuration of the line, and the natural tendency of the line to adopt a twist configuration ($\Phi = \pi/2$) as mentioned earlier. It is described by the angle $\Phi(z, r)$ which increases monotonically from zero at the meniscus to a finite value at the defect loop. At a radius r between R_l and R_g, the function $\Phi(z, r)$ is maximal in the midplane ($z = 0$) and decreases symmetrically towards the glass plates ($z = \pm d/2$) to a finite value. Then a small twist deformation appears along z.

If the ratio R_l/R_g is small, the influence of the anchoring at the meniscus on the structure of the line is weak. Then one can assume that the value $\Phi(0, R_l)$ is $\pi/2$ and the line is in a twist configuration, figure 4 (*b*). Experimental observations confirm this idea. But for larger values of R_l/R_g this cannot be assumed and experimental observations did not allow us to determine $\Phi(0, R_l)$ precisely.

We measured the opening angle (α) of the extinction brushes (see figure 6) as a function of the loop radius. α decreases linearly with increasing R_l indicating the change of the director configuration as the width of the deformed zone $R_g - R_l$ decreases. There is a cross over to a regime (at about 30 μm for this globule) with a stronger dependence on the line radius (a larger slope of the $\alpha(R_l)$ function) when the defect line approaches the meniscus. This behaviour is similar for any globule radius R_g. The cross over always occurs at a distance from the meniscus of the order of its thickness M. We conclude that this is linked to details of the meniscus shape and the anchoring conditions.

Supposing that the polarization of the light follows exactly the variations of the angle $\Phi(z, r)$, α is then a measure of $\Phi(\pm d/2, R_l)$. But in fact, because the angle $\theta(z)$ is a function of z, the polarization cannot rotate around z as fast as the director. Then we have $\Phi(\pm d/2, R_l) \leqslant \alpha \leqslant \Phi(0, R_l) \leqslant \pi/2$. Then, for values between 0 and $\pi/2$, α is always slightly greater than $\Phi(\pm d/2, R_l)$ except in the case $\alpha = \pi/2$ for which there is no twist along z because $\Phi(z, R_l)$ cannot be different from $\pi/2$.

Further experimental evidence of the twisted nature of the line is given by the appearance of point defects (cusps) observed along the line. It has been shown [16] that in (uniaxial) nematics, when the director orientation in the region of the π wall forces the director to be perpendicular to the twisted line in the midplane of the sample, the line can exhibit cusps. The two energetically equivalent orientations, one on one side and one on the other side of the cusp ('zig' and 'zag'), correspond to the two possible directions in which the director can

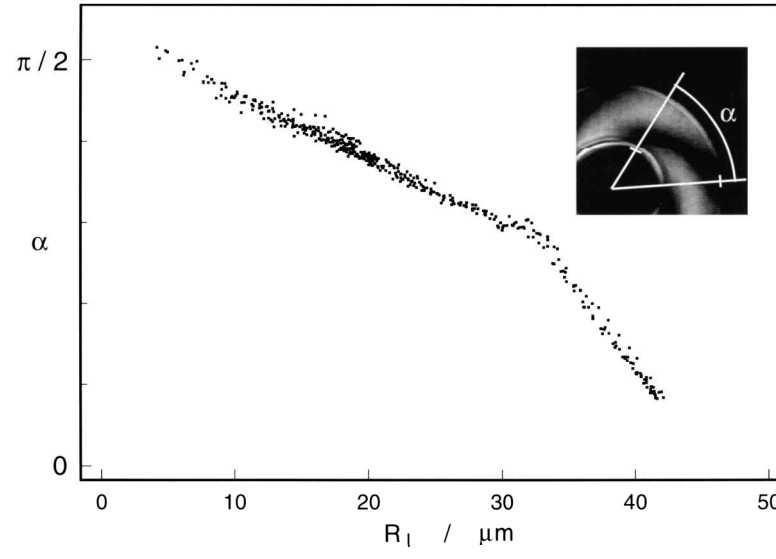

Figure 6. Opening angle of the brushes α (defined in the inserted picture) is measured as a function of the position of the line.

escape along the line axis. Two successive segments of a line are then separated by a cusp where locally the line is of the wedge type [4].

In our experiments, the defect line usually appeared with several cusps (always an even number) which deform the loop and break its cylindrical symmetry. To restore this symmetry by annihilating the cusps, we used a slowly rotating (few Hz) magnetic field in the plane of the glass plates. A small asymmetry of the magnetic field forces the cusps to approach each other, and leads to their annihilation after a few tens of seconds. Finally we obtain a cylindrically symmetric system, see figure 2(*a*): there is a unique escape direction along the line. Depending on the direction of the rotation of the magnetic field, the spiral shape of the extinction brushes is right- or left-handed.

4. Theoretical considerations: condition of the line equilibrium

In this section we introduce characteristic quantities in terms of which we will later present and analyse the experimental results. We give an expression for the free energy density of the globule, taking into account elastic and electric contributions, as well as terms accounting for the line tension of the defect and for its interaction with the meniscus. After some approximations we minimize the total free energy density in order to find the critical (unstable equilibrium) defect loop radius.

4.1. *Free energy*

The free energy F of the system can be written in the form:

$$F = F_l + F_d + F_h + F_m \tag{1}$$

where F_l is the energy of the loop which is in competition with the deformation energy F_d of the reversal domain containing the π wall, and F_h is the electric contribution to the energy in the homeotropic central region. These terms model the situation of a wedge line sufficiently. In case of a twisted line, in our geometry, one needs to have an additional term F_m to characterize the interaction of the line with the meniscus, taking into account the out-of-plane director component (azimuthal angle Φ). F_m should be a function of $R_g - R_l$ in such a way that F_m increases with R_l for a given R_g.

The free energy, equation (1), leads to the existence of an unstable equilibrium position of the line at a critical radius $R_l^c(V, R_g)$ above which the loop will grow, and below which it will shrink and the reversal domain will occupy the whole globule. $R_l^c(V, R_g)$ is a function of the applied voltage V and the globule radius.

The exact director distribution is hard to calculate and a simple model is introduced in order to estimate the energy of the system. We assume that the director is parallel to z (homeotropic alignment) in the region $r < R_l$. In the reversal domain for $R_l < r < R_g$ we assume $\theta(z)$ to be independent of r. This means that we simplify the exact director distribution close to the line, and introduce a singularity in the spatial derivative of the vector $\mathbf{n}$ at $r = R_l$. We may assume that the energy is not affected strongly by such an approximation. Moreover, the distribution close to the line is taken into account in the term F_l.

4.1.1. *Line energy*

In this model we do not go into the details of the line energy; we suppose the energy density per unit length σ to be independent of the field applied. The line energy is:

$$F_l = 2\pi R_l \sigma. \tag{2}$$

4.1.2. *Electric energy and deformation energy of the reversal domain*

We will make the assumption that the deformation energy of the reversal domain is composed of two independent terms. The first one comes from the distortion along the vertical z-axis. The second one originates from the distortion in the plane (r, ψ) and is due to the curvature in such a cylindrical system. This second contribution will be taken into account in the F_m term and we will restrict F_d to the first elastic contribution and to the electric energy. Then F_d can be expressed as the product of the total surface of the reversal domain and the energy density per unit area, which we call Δu.

$$F_d = \pi(R_g^2 - R_l^2)\Delta u. \tag{3}$$

In order to calculate Δu, we approximate $\theta(z)$ by the one-dimensional problem of the π-wall ($\Phi = 0$). The director is described by:

$$\mathbf{n} = \begin{cases} \sin\theta(z) \\ 0 \\ \cos\theta(z) \end{cases}$$

The free energy density [17] is then given by:

$$f_d = \frac{K_1}{2}(\operatorname{div}\mathbf{n})^2 + \frac{K_3}{2}(\mathbf{n}\times\operatorname{curl}\mathbf{n})^2 - \frac{\varepsilon_o\varepsilon_a}{2}(\mathbf{E}\ \ \mathbf{n})^2$$

$$= \frac{K_3}{2}[1 - k^2\sin^2\theta(z)]\left[\frac{\partial}{\partial z}\theta(z)\right]^2 - \frac{\varepsilon_o\varepsilon_a}{2}E^2\cos^2\theta(z) \tag{4}$$

with

$$k^2 = \frac{K_3 - K_1}{K_3} > 0$$

The Euler–Lagrange equation

$$\frac{\mathrm{d}}{\mathrm{d}z}\left\{\frac{\partial f_\mathrm{d}}{\partial[\partial\theta(z)/\partial z]}\right\}=\frac{\partial f_\mathrm{d}}{\partial\theta(z)} \tag{5}$$

gives:

$$\sin\theta(z)\cos\theta(z)\left\{k^2\left[\frac{\partial}{\partial z}\theta(z)\right]^2+m^2\right\}$$
$$=[1-k^2\sin^2\theta(z)]\left[\frac{\partial^2}{\partial^2 z}\theta(z)\right] \tag{6}$$

where

$$m=\left(\frac{\varepsilon_\mathrm{o}\,\varepsilon_\mathrm{a}}{K_3}\right)^{1/2}\frac{V}{d}>0$$

and V is the applied voltage.

Equation (6) can be solved simply when there is no electric field ($m=0$) or in the case of the one-constant approximation ($k=0$).

In the case of $m=0$, taking into account the boundary conditions $z(\theta=0)=\pm d/2$ and the condition $z(\theta=\pi/2)=0$ obtained by symmetry, the solution of equation (6) is:

$$z(\theta)=\pm\frac{d}{2}\left[1-\frac{L_\mathrm{E}(\theta,k)}{L_\mathrm{E}(\pi/2,k)}\right] \tag{7}$$

and the free energy density integrated along the z-axis is:

$$\Delta u=\frac{K_3}{2}\frac{4L_\mathrm{E}^2(\pi/2,k)}{d} \tag{8}$$

where $L_\mathrm{E}(\theta,k)$ is the Legendre elliptic integral of second rank.

When an electric field is applied ($m\neq 0$), we take $K_1=K_3=K$ ($k=0$) in order to find an analytic solution which leads to:

$$z(\theta)=\pm\frac{d}{2}\frac{L_\mathrm{F}(\pi/2-\theta,h)}{L_\mathrm{F}(\pi/2,h)} \tag{9}$$

and

$$\Delta u=\frac{K}{2}\frac{4L_\mathrm{F}(\pi/2,h)}{d}[2L_\mathrm{E}(\pi/2,h)-L_\mathrm{F}(\pi/2,h)] \tag{10}$$

where $L_\mathrm{F}(\theta,k)$ is the Legendre elliptic integral of first rank and h, called generally the modulus, depends on the applied field and is the solution of the equation:

$$hL_\mathrm{F}(\pi/2,h)=m\frac{d}{2}. \tag{11}$$

h takes its limiting values 0 and 1 for zero and infinitely high electric fields, respectively. This equation expresses the condition $\theta=\pi/2$ at the midplane $z=0$.

4.1.3. *Electric energy of the homeotropic domain*

Using the same notations indicated earlier we write:

$$F_\mathrm{h}=-\frac{K}{2}\pi R_1^2 m^2 d. \tag{12}$$

4.1.4. *Interaction of the line with the meniscus*

The interaction of the line with the meniscus is the most complicated term to describe. Some simplifications have to be made to approximate F_m. We suggest making an analogy with 'the magic spiral' problem [2] which describes the director distribution in a nematic enclosed between two concentric cylinders with different boundary conditions on their surface. The 2-dimensional [(r,ψ) dependence] case has the solution:

$$\Phi(r)=(\pi/2)\ln(r/R_\mathrm{g})/\ln(R_1/R_\mathrm{g}). \tag{13}$$

This situation is similar to the one we have in our problem in the plane at $z=0$.

It is important to note that F_m is field dependent. When the electric field is applied the turn over region gets thinner along z. F_m, which is also the result of integration along z, then becomes lower.

An estimation of F_m is possible starting from the Φ-distribution given by equation (13). We assume strong perpendicular anchoring at the air interface [11]. The main hypothesis is that we suppose $\Phi(z,r)=\Phi(0,r)$ given by equation (13) for any z. This means that we neglect the twist deformation along z or forget that the line has, on a microscopic scale, the structure drawn in figure 4(*b*). This estimation gives:

$$F_\mathrm{m}=\pi K D(V)\left[\frac{(\pi/2)^2+\ln^2(R_\mathrm{g}/R_1)}{\ln(R_\mathrm{g}/R_1)}\right] \tag{14}$$

where $D(V)$ is a measure of the thickness of the turn over region along z:

$$D(V)=\int_{-d/2}^{d/2}\sin^2\theta(z)\,\mathrm{d}z$$
$$=\frac{d}{h^2}\left[\frac{L_\mathrm{E}(\pi/2,h)}{L_\mathrm{F}(\pi/2,h)}-(1-h^2)\right]. \tag{15}$$

$D(V)$ tends to $d/2$ for $V\to 0\,(h\to 0)$ and approaches the electric coherence length $\xi=(K_3/\varepsilon_\mathrm{o}\,\varepsilon_\mathrm{a})^{1/2}(d/V)$ [2] at high field ($h=1$).

The R_1-derivative of F_m is:

$$\frac{\partial F_\mathrm{m}}{\partial R_1}=\pi K D(V)\frac{(\pi/2)^2-\ln^2(R_\mathrm{g}/R_1)}{R_1\ln^2(R_\mathrm{g}/R_1)}. \tag{16}$$

Equation (16) shows that when the line gets closer to the meniscus, the in-plane splay–bend deformation become greater. And when the radius of the line decreases, the bend deformation close to the line is more and more important and the energy diverges at $R_1=0$. Then this

leads to the existence of a minimum of F_m between $R_l = 0$ and $R_l = R_g$. This corresponds to $R_l/R_g = \exp(-\pi/2) \simeq 0.2$. For R_l greater than $0.2R_g$, the force acting on the line is repulsive, in the case of $R_l < 0.2R_g$ it becomes attractive.

4.2. *Critical radius*

For large R_g (or small R_g but sufficiently high electric field) the total energy F has two minima, one at R_l close to zero and the other close to R_g. Depending on the globule size and the electric field, the absolute minimum can be one or the other. Between these two minima, the free energy reaches a maximum value at a line radius called the critical radius R_l^c.

For low values of R_g and a low electric field, the second minimum disappears because of the dominating repulsion term, equation (14). This means that the line spontaneously shrinks. When R_l^c does exist, the R_l-derivative of F gives the solution for R_l^c. Three cases can be considered.

(1) *When the interaction of the line with the meniscus is negligible* ($R_l^c \simeq 0.2R_g$), the critical radius can be given by the function:

$$R_l^{no\,m}(V) = \frac{(d/2)(\sigma/K)}{L_F(\pi/2, h)[2L_E(\pi/2, h) - (1 - h^2)L_F(\pi/2, h)]}. \tag{17}$$

The two limiting cases are:

V_{LC}/V is small ($h = 1$), then $R_l^{no\,m}(V)$ is proportional to $(1/V)$;

V_{LC}/V is large ($h = 0$), then the critical radius saturates at a constant value of $R_l^{no\,m}(V) = R_l^{no\,m}(0) = (d/2)(\sigma/K)/(\pi/2)^2$ (figure 7 shows curves calculated for 5CB).

$V_{LC} = 2(K/\varepsilon_0\varepsilon_a)^{1/2}$ is a material parameter. This can also be used to estimate experimentally the line tension σ of the defect (in units of the elastic constant); this resulted in a value of $\sigma = 8.4K$ in our case.

The limit $R_l^{no\,m}(0)$ can be estimated much more accurately by taking into account the anisotropy of the elastic constants; thus $k \neq 0$:

$$R_l^{no\,m}(0) = \frac{(d/2)(\sigma/K_3)}{L_E^2(\pi/2, k)}. \tag{18}$$

In figure 7, the critical line radius is plotted as a function of the relative voltage. The lowest curve in figure 7, calculated for $R_g = 135\,\mu m$, corresponds to the *no interaction* case and is given by equation (18).

(2) *In the general case*, also taking into account the *interaction term*, the cancelling of the first R_l-derivative of F gives:

$$R_l = R_l^{no\,m}(V)\left[1 + \frac{1}{2\pi\sigma}\left(\frac{\partial F_m}{\partial R_l}\right)_{Rl}\right]. \tag{19}$$

The critical radius R_l^c is the solution $R_l = R_l^c$ of this equation and can be checked numerically.

The high voltage (linear) part of the curve (figure 7) remains unaffected by the *interaction term* for any globule radius, but the zero voltage limit of R_l^c shifts to higher values as R_g decreases (e.g. the curves for $R_g = 83$, and $R_g = 51\,\mu m$ in figure 7). Both terms on the rhs of equation (19) contribute and one observes an 'S' shape of the curve (see the results for $R_g = 35$, 40 and 47 μm in figure 7).

(3) *The tricritical limit*. As mentioned earlier, for small R_g, the critical radius does not exist above a certain value of the electric field because the repulsion term is

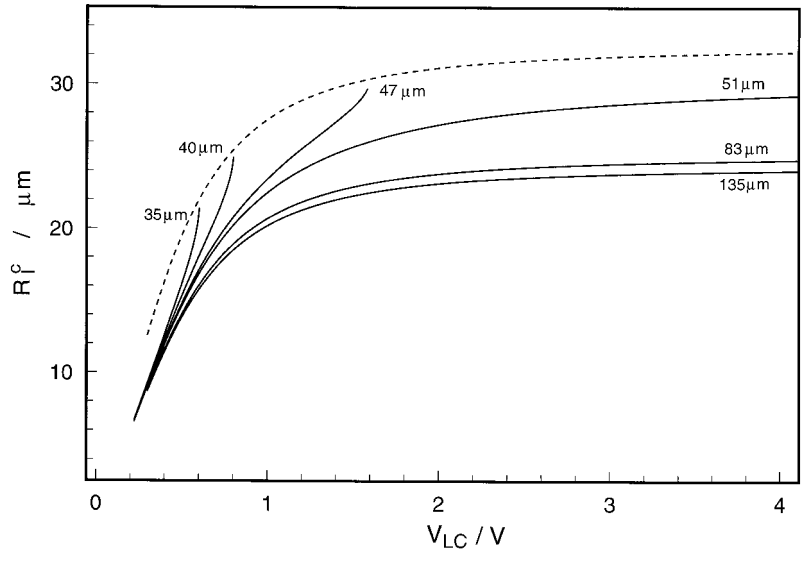

Figure 7. Theoretical prediction of the critical radius for different globule sizes as a function of the inverse of the applied voltage (using $\sigma = 8.4K$), $R_g = 35$, 40, 47, 51, 83 and 135 μm. The dashed line is the tricritical limit. $V_{LC} = 2(K/\varepsilon_o\varepsilon_a)^{1/2}$ is a material parameter. $R_l^{norep}(V = 0) = 24.5\,\mu m$.

dominant. One can calculate the minimum electric field for which R_l^c still exists. This occurs at that voltage where the energy maximum and minimum coincide; thus the first and second derivatives of the energy simultaneously vanish. One has to solve a system consisting of equations (19) and (20), the latter equation is obtained by direct derivation of equation (19):

$$R_l^{nom}(V)\frac{1}{2\pi\sigma}\left(\frac{\partial^2 F_m}{\partial R_l^2}\right)_{Rl=Rl^c(V,Rg)}=1. \qquad (20)$$

The solution of this system is a tricritical point in the parameter space (V, R_g, R_l^c) and will be denoted by (V_o, R_{go}, R_{lo}^c).

The solution (V_o, R_{go}, R_{lo}^c) delivers the dashed line shown in figure 7 and the nearly constant part of the curve for low R_g in figure 8, where black dots represent the experimental data for the tricritical behaviour. Figure 8 also shows the solution of equation (19) for $V=0$ (globule radii above 50 μm) and the corresponding experimental results (circles).

Solutions of equation (19) for different values of R_g (full lines), and the solution of the system of equations (19, 20) (dashed line) are shown in figure 7.

5. Comparison of experiments and theory

Most of our measurements were made for a thickness $d=14.5\pm0.5$ μm. It was found that at zero voltage the largest globule which had the point defect ($R_l=0$) as the stable configuration was $R_g=47$ μm. The smallest one, which had the defect line close to the meniscus as the stable configuration, was $R_g=51$ μm. We assume, that the experimental value of $R_{go}(V_o=0)$ is 49 ± 2 μm. This is in a very good agreement with the theoretically predicted value which is 50.1 μm and can be deduced from figure 8. It corresponds to the cross over of the theoretical curve from its approximately constant part (tricritical range without stationary line radius) to the rapidly decreasing part, where the critical radius is given by equation (19) (for $V=0$). We note, that the experimental points (black dots in figure 8) obtained for globules in the range 20 μm$< R_g <$ 47 μm (with a stable point defect configuration) in such a way, that the minimum voltage was measured at which the loop defect could be stabilized, show also a cross over around 50 μm. This is an independent measurement from the observation of the stable globule configuration without electric field. The experimental data for R_l^c/R_g in this R_g region (below 50 μm) scatter within 0.68 ± 0.02 which is a range determined by the experimental accuracy. The model (continuous line) predicts a slight increase of R_l^c/R_g with R_g reaching a value of 0.65 at the crossover. This discrepancy could be due to the approximation used for determination of the interaction term (F_m) between the line and the meniscus.

On the right side of figure 8, $R_l^c(0, R_g)/R_g$ versus R_g is presented for globules larger than R_{go}. $R_l^c(0, R_g)/R_g$ tends to the value $24.5/135\simeq0.2$ in the R_g range studied (50 μm … 135 μm). In this range, the force due to the in-plane deformation, derived from equation (16), is always repulsive. As was discussed before, if the value of R_l^c is of the order of $0.2R_g$, the repulsive force acting on the line is zero. This is the case for $R_g=135$ μm because $R_l^c(0, 135)=24.5$ μm. This value gives $R_l^{nom}(V=0)$ which can be given either by equations (17) or (18), depending on whether the anisotropy of the elastic constants is taken into account.

We measured the critical radius as a function of the applied voltage for several globule sizes R_g in a range including $R_{go}(V=0)$. Results obtained are shown in figure 9. The asymptotic limits for low $1/V$

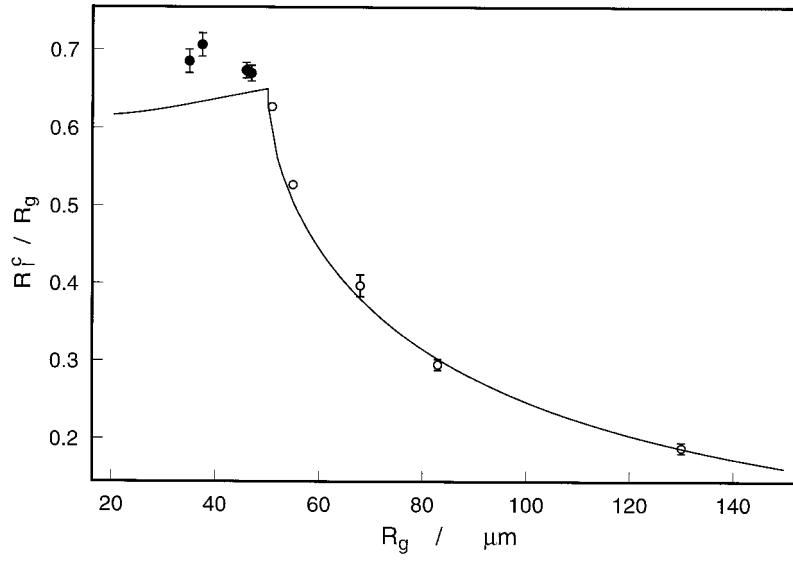

Figure 8. Experimental measurements and model prediction (using $\sigma=8.4K$) of the tricritical range (left part, black dots) and critical radius at zero field applied (right part, white dots). Experimentally, the tricritical point at $V_o=0$ is obtained for $R_l^{co}=49\pm2$ μm, theoretically for $R_l^{co}=50.1$ μm, $d=14.5$ μm.

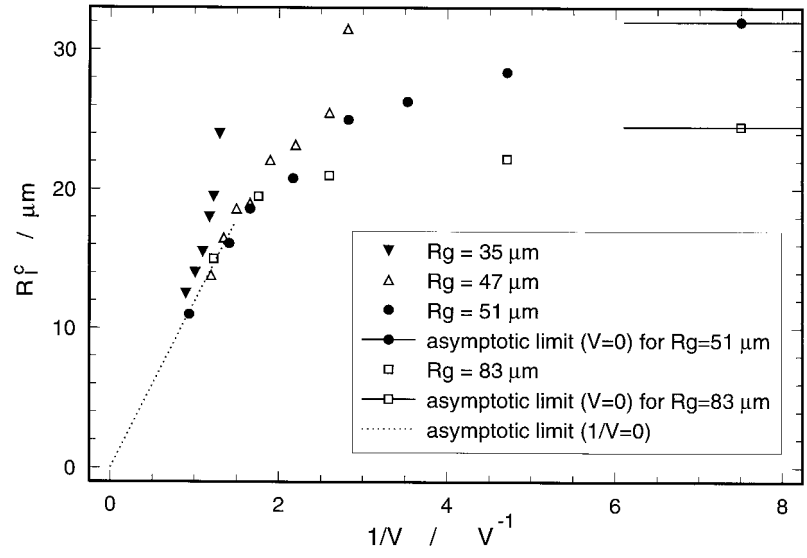

Figure 9. Experimental measurements of the critical radius for different globule radii as a function of the inverse of the applied voltage, $d = 14.5\,\mu m$.

[dotted line, given by equation (19)] and for high $1/V$ [continuous lines calculated for $R_g = 51\,\mu m$ and $83\,\mu m$ from equation (19)] are also shown. A good qualitative agreement can be seen between theory and experiment by comparing figures 7 and 9. Experiments show the saturating behaviour in the limit of large $1/V$ for $R_g > R_{go}$.

For $R_g = 135\,\mu m$ and $V = 0$, the interaction with the meniscus vanishes and the asymptotic value for the R_l^c can be calculated from equations (17) and (18). For medium globules ($R_g = 51\,\mu m$ and $83\,\mu m$) this is not the case and $R_l^c(0, R_g)$ shifts to higher values as predicted by equation (19), and can also be seen experimentally. For smaller globules (see $R_g = 35\,\mu m$ and $47\,\mu m$) the 'S' shape can also be clearly seen. There are quantitative deviations especially for $R_g < R_{go}$. The exact 'S' shape of the curve is basically determined by the force of the interaction energy (F_m) which we approximated by equation (16). By describing it more precisely one could expect a better quantitative agreement.

As already mentioned, our model allows us to determine the line tension (σ) of the loop defect. Using equation (17) for the isotropic elasticity we obtain $\sigma = (8.4 \pm 0.3)K$ and using equation (18), taking into account anisotropy, we have $\sigma = (7.3 \pm 0.3)K_3$ taking $k^2 = 0.23$.

In the calculations presented we used the value of $8.4K$. In order to check whether this is a realistic value we compared it with other work [3]. Ranganath [3] has calculated the free energy of the planar twist deformation per unit length of a defect line, using the approximation $K_1 = K_3 = K$:

$$f_{twist} = \frac{\pi}{4}(KK_2)^{1/2} \ln(l/\alpha) + f_{twist}^{core} \qquad (21)$$

where the diameter of the core α is $\sim 100\,Å$ and the energy per unit length of the core f_{twist}^{core} is estimated $\sim (KK_2)^{1/2}/2$. In our model we did not go into the details of this energy which is supposed to vary with the thickness l of the turn over region, which itself is electric field dependent. Because l appears in f_{twist} through a logarithmic term, it does not lead to significant modifications in the electric field range used. Then, considering σ as a constant value seems to be a good approximation. Calculation from equation (21) gives $f_{twist} \sim 6$–$7\,K$, with typically $l \sim 15\,\mu m$.

6. Conclusion

Analysis of the extinction brushes permits one to understand the director distribution around a twisted line constrained in the plane of the sample. This kind of line is most commonly found in nematic liquid crystals because the elastic constants usually verify the Anisimov and Dzyaloshinskii [14] condition for the stability of a wedge disclination (see §3.2).

We estimated the force acting on the line due to the in-plane elastic deformation and found qualitatively good agreement with the experiments. We have measured the tension of a twisted line in the case of 5CB in a sample of thickness $d = 14.5 \pm 0.5\,\mu m$ and compared the results with the prediction made by Ranganath [3] and found satisfactory agreement.

Our experiment also permits us to observe the transformation from a loop line defect to a topologically equivalent point defect. The inverse transformation can also be carried out by using a very high electric field. This process is of high interest and the mechanism of this transformation is the subject of experimental and theoretical work that is in progress. These observations

are related to the theoretical work done by the authors of reference [18]. The question raised is whether a point defect could be energetically unstable against expanding into a ring disclination of small radius. The nature of the transition defect–extended loop defect should be different in the case of a real point defect or small radius ring defect. Attention will be devoted to this transition experimentally in different liquid crystals in the near future.

We would like to thank Lorenz Kramer and Maurizio Nobili for fruitful discussions. This work has been done with financial support of the DRET administration (94-2610A). A.B. wishes to thank the hospitality of the INLN. Financial support of the CNRS-OMFB F-2/98, the EU TMR FMRX-CT96-0085 and the OTKA T-014957 is acknowledged.

References

[1] KLEMAN, M., 1983, *Lines and Walls in Liquid Crystals, Magnetic Systems and Various Ordered Media* (New York: Wiley).

[2] DE GENNES, P. G., and PROST, J., 1993, *The Physics Of Liquid Crystals* (Oxford: Clarendon Press).

[3] RANGANATH, G. S., 1982, *Mol. Cryst. liq. Cryst.*, **87,** 187.

[4] CHANDRASEKHAR, S., and RANGANATH, G. S., 1986, *Adv. Phys.*, **35,** 507.

[5] LEGER-QUERCY, L., 1976, PhD thesis, Université de Paris-Sud, France; HELFRICH, W., 1968, *Phys. Rev. Lett.*, **21,** 1518; WILLIAMS, R., 1968, *Phys. Rev. Lett.*, **21,** 342; BROCHARD, F., 1972, *J. Physique*, **33,** 607; FRISCH, T., COULLET, P., RICA, S., and GILLI, J. M., 1994, *Phys. Rev. Lett.*, **72,** 1471.

[6] GILLI, J. M., THIBERGE, S., VIERHEILIG, A., and FRIED, F., 1997, *Liq. Cryst.*, **23,** 619.

[7] MINOURA, K., KIMURA, Y., ITO, K., and HAYAKAWA, R., 1997, *Mol. Cryst. liq. Cryst.*, **302,** 345; PARGELLIS, A. N., GREEN, S., and YURKE, B., 1994, *Phys. Rev. E*, **49,** 4250; PARGELLIS, A. N., FINN, P., GOODBY, J. W., PANIZZA, P., YURKE, B., and CLADIS, P., 1992, *Phys. Rev. A*, **46,** 7765; PLEINER, H., 1988, *Phys. Rev. A*, **37,** 3986; LAVRENTOVICH, O. D., and PERGAMENSHCHIK, V. M., 1995, *Int. J. mod. Phys. B*, **9,** 251.

[8] CLADIS, P., VAN SARLOOS, W., FINN, P. L., and KORTAN, A. R., 1987, *Phys. Rev. Lett.*, **58,** 222.

[9] BECHOEFER, J., 1988, PhD thesis, University of Chicago, USA.

[10] LAVRENTOVICH, O. D., KLEMAN, M., and PERGAMENSHCHIK, V. M., 1994, *J. Phys. II Fr.*, **4,** 377.

[11] COGNARD, J., 1981, *Mol. Cryst. liq. Cryst.*, **76,** Supl. 1, 1.

[12] See for example, HARTSHORNE, N. H., and STUART, A., 1970, *Crystals and the Polarizing Microscope*, 4th Edn (London: Edward Arnold Publishers).

[13] PRESS, M. J., and ARROTT, A. S., 1995, *J. Phys. (Paris)*, **36,** C1-177.

[14] ANISIMOV, S. I., and DZYALOSHINSKII, I. E., 1973, *Sov. Phys. JETP*, **36,** 774.

[15] $K_1 = 6.5$, $K_2 = 3.0$, $K_3 = 9.0 \times 10^{-12}$ N^{-1}: BUNNING, J. D., FABER, T. E., and SHERRELL, P. L., 1981, *J. Physique*, **42,** 1175.

[16] GALERNE, Y., ITOUA, J., and LIÉBERT, L., 1988, *J. Phys. Fr.*, **46,** 681.

[17] FRANK, F. C., 1958, *Disc. Faraday Soc.*, **25,** 19.

[18] MORI, H., and NAKANISHI, H., 1988, *J. Phys. Soc. Jpn.*, **57,** 1281; LAVRENTOVICH, O. D., ISHIKAWA, T., and TERENTJEV, E. M., 1997, *Mol. Cryst. liq. Cryst.*, **299,** 301.